PHYSICAL REVIEW D **90,** 094506 (2014)

Nature of Roberge-Weiss transition endpoints for heavy quarks in $N_f = 2$ lattice QCD with Wilson fermions

Liang-Kai Wu*

Faculty of Science, Jiangsu University, Zhenjiang 212013, People's Republic of China

Xiang-Fei Meng

National Supercomputer Center, Tianjin 300457, People's Republic of China

(Received 10 May 2014; revised manuscript received 4 September 2014; published 18 November 2014)

The phase structure of QCD with imaginary chemical potential provides information on the phase diagram of QCD with real chemical potential. With imaginary chemical potential $i\mu_I = i\pi T$, previous studies show that the Roberge-Weiss (RW) transition endpoints are triple points at both large and small quark masses, and second order transition points at intermediate quark masses. The triple and second order endpoints are separated by two tricritical ones. We present simulations with $N_f = 2$ Wilson fermions to investigate the nature of RW transition endpoints. The simulations are carried out at 8 values of the hopping parameter κ ranging from 0.020 to 0.140 on different lattice volumes. The Binder cumulant, susceptibility, and reweighted distribution of the imaginary part of the Polyakov loop are employed to determine the nature of RW transition endpoints. The simulations show that the two tricritical points are within the ranges 0.070–0.080 and 0.120–0.140, respectively.

DOI: 10.1103/PhysRevD.90.094506 PACS numbers: 12.38.Gc, 11.10.Wx, 11.15.Ha, 12.38.Mh

I. INTRODUCTION

The study of QCD phase diagram is of great importance theoretically and phenomenologically; overviews may be found in Refs. [1,2] and references therein. On and below the scales of a baryon mass which is relevant to heavy ion collision and astrophysics, the nonperturbative nature of QCD warrants the Monte Carlo (MC) simulation of lattice QCD. Although substantial progress has been achieved at zero baryon density, the MC simulation of lattice QCD is accompanied by the "sign" problem when studies are extended to finite density, for example, see Ref. [3]. To date, many indirect methods have been proposed to circumvent the sign problem; overviews with references to these methods can be found in Refs. [3,4]. One of these methods consists of simulating QCD with imaginary chemical potential for which the fermion determinant is positive [5–13].

QCD with imaginary chemical potential has a rich phase structure, and it not only deserves detailed investigation in its own right theoretically, but also has significant relevance to physics at zero or small real chemical potential [5–8,14–18]. The tricritical line found at the imaginary chemical potential, with its associated scaling law, imposes constraints on the phase diagram of QCD at real chemical potential [5].

The partition function of QCD with complex chemical potential has two important symmetries [19]: reflection symmetry in $\mu = \mu_R + i\mu_I$ and periodicity in imaginary chemical potential. The $Z(3)$ symmetry is explicitly broken at the presence of dynamical quarks for real chemical potential. However, for complex μ, due to the periodicity of partition function in imaginary chemical potential, the $Z(3)$ symmetry is restored. Different $Z(3)$ sectors are distinguished by the Polyakov loop. Transition between adjacent $Z(3)$ sectors in μ_I is analytic for low temperature, and is of first order [Roberge-Weiss (RW) transition] for high temperature. The first order transition that takes place at critical values of the imaginary chemical potential $\mu_I/T = (2n+1)\pi/3$ [19–21] forms a transition line, thus the first order transition line in the high temperature region necessarily ends at an endpoint T_{RW} when the temperature is decreased sufficiently low.

Recent numerical studies [5–7] show that the RW transition endpoints are triple points for small and heavy quark masses, and second order points for intermediate quark masses. So there exist two tricritical points separating the first order transition points from the second ones. Moreover, it is pointed out [5,17,18] that the scaling behavior at the tricritical points may shape the critical line which separates different transition regions for real chemical potential, and thus, the critical line for real chemical potential is expected to be qualitatively consistent with the scenario suggested in Refs. [11,12] which show that the first order transition region shrinks with increasing real chemical potential.

Most of studies for finite density QCD have been performed using staggered fermion action or the improved versions. The disadvantages of staggered fermion discretization [22–24] warrants studies of lattice QCD with a different discretization. In Refs. [25,26], Wilson fermion is employed to investigate the nature of the RW transition

*Corresponding author.
wuliangkai@163.com

endpoints, but the κ values in Ref. [26] are limited from 0.155 to 0.198.

In this paper, proceeding with our previous work [26] along this direction, we attempt to investigate the RW transition line endpoints with $N_f = 2$ Wilson fermions with κ ranging from 0.020 to 0.140. In Sec. II, we define the lattice action with imaginary chemical potential and the physical observables we calculate. Our simulation results are presented in Sec. III followed by discussions in Sec. IV.

II. LATTICE FORMULATION WITH IMAGINARY CHEMICAL POTENTIAL

We consider a system with $N_f = 2$ degenerate Wilson fermions whose partition function with chemical potential is

$$\begin{aligned} Z &= \int [dU][d\bar{\psi}][d\psi] e^{-S_g - S_f} \\ &= \int [dU] (\mathrm{Det}M[U,\theta])^{N_f} e^{-S_g}, \end{aligned} \tag{1}$$

where S_g is the gauge action, and S_f is the quark action with the quark imaginary chemical potential $\mu_I = \theta T$. For S_g, we use the standard one-plaquette action

$$S_g = \beta \sum_p \left(1 - \frac{1}{N_c} \mathrm{ReTr} U_p\right), \tag{2}$$

where $\beta = 6/g^2$, and the plaquette variable U_p is the ordered product of link variables U around an elementary plaquette. For S_f, we use the standard Wilson action

$$S_f = \sum_{f=1}^{N_f} \sum_{x,y} \bar{\psi}_f(x) M_{x,y}(U,\kappa,\mu) \psi_f(y), \tag{3}$$

where κ is the hopping parameter, related to the bare quark mass m and lattice spacing a by $\kappa = 1/(2am + 8)$. The fermion matrix is

$$\begin{aligned} M_{x,y}(U,\kappa,\mu) = \delta_{x,y} &- \kappa \sum_{j=1}^{3} [(1-\gamma_j) U_j(x) \delta_{x,y-\hat{j}} \\ &+ (1+\gamma_j) U_j^{\dagger}(x-\hat{j}) \delta_{x,y+\hat{j}}] \\ &- \kappa [(1-\gamma_4) e^{a\mu} U_4(x) \delta_{x,y-\hat{4}} \\ &+ (1+\gamma_4) e^{-a\mu} U_4^{\dagger}(x-\hat{4}) \delta_{x,y+\hat{4}}]. \end{aligned} \tag{4}$$

We carry out simulations at $\theta = \pi$. As it is pointed out, the system is invariant under the charge conjugation at $\theta = 0, \pi$, when θ is fixed [16]. But the θ-odd quantity $O(\theta)$ is not invariant at $\theta = \pi$ under charge conjugation. When $T < T_{RW}$, $O(\theta)$ is a smooth function of θ, so it is zero at $\theta = \pi$. Whereas when $T > T_{RW}$, the two charge violating solutions cross each other at $\theta = \pi$. Thus, the charge symmetry is spontaneously broken there and the θ-odd quantity $O(\theta)$ can be taken as an order parameter. In this paper, we take the imaginary part of the Polyakov loop as the order parameter.

The Polyakov loop L is defined as the following:

$$\langle L \rangle = \left\langle \frac{1}{V} \sum_{\mathbf{x}} \mathrm{Tr} \left[\prod_{t=1}^{N_t} U_4(\mathbf{x}, t) \right] \right\rangle, \tag{5}$$

here and in the following, V is the spatial lattice volume. To simplify the notations, we use X to represent the imaginary part of the Polyakov loop L, $X = \mathrm{Im}(L)$.

The susceptibility of the imaginary part of the Polyakov loop χ is defined as

$$\chi = V \langle (X - \langle X \rangle)^2 \rangle, \tag{6}$$

which is expected to scale as [6,7]

$$\chi = L_s^{\gamma/\nu} \phi(\tau L_s^{1/\nu}), \tag{7}$$

where τ is the reduced temperature $\tau = (T - T_{RW})/T_{RW}$, $V = L_s^3$. This means that the curves $\chi/L_s^{\gamma/\nu}$ at different lattice volume should collapse with the same curve when plotted against $\tau L_s^{1/\nu}$. In the following, we employ $\beta - \beta_{RW}$ in place of $\tau = (T - T_{RW})/T_{RW}$. The critical exponents relevant to our study are collected in Table I [7,27].

We also consider the Binder cumulant of the imaginary part of the Polyakov loop which is defined as the following:

$$B_4 = \langle (X - \langle X \rangle)^4 \rangle / \langle (X - \langle X \rangle)^2 \rangle^2, \tag{8}$$

TABLE I. Critical exponents relevant to our study.

	ν	γ	γ/ν
3D ising	0.6301(4)	1.2372(5)	1.963
Tricritical	1/2	1	2
First order	1/3	1	3

TABLE II. Results of critical couplings β_{RW} on different spatial volumes at different κ.

κ	8	12	16	20
0.020	5.695(20)	5.697(14)	5.691(7)	5.684(10)
0.040	5.706(19)	5.694(12)	5.688(9)	5.693(6)
0.060	5.725(25)	5.691(8)	5.687(7)	5.689(6)
0.070	5.712(21)	5.690(9)	5.695(5)	5.693(6)
0.080	5.713(25)	5.687(13)	5.683(7)	5.684(5)
0.100	5.672(14)	5.659(6)	5.687(4)	5.688(3)
0.120	5.618(12)	5.650(7)	5.619(3)	5.609(5)
0.140	5.639(21)	5.636(21)	⋯	⋯

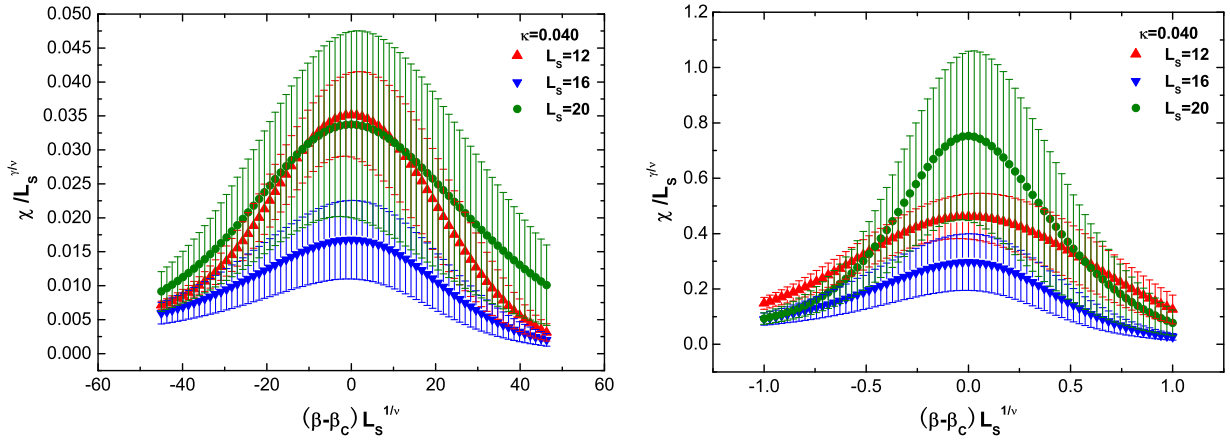

FIG. 1 (color online). Scaling behavior of the susceptibility of the imaginary part of the Polyakov loop according to the first order critical index (left panel), and to the 3D Ising critical index (right panel) at $\kappa = 0.040$.

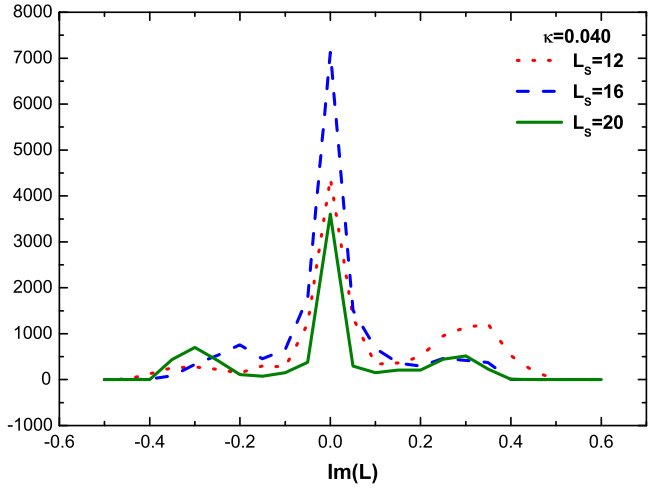

FIG. 2 (color online). Reweighted distribution of the imaginary part of the Polyakov loop at $\kappa = 0.040$ at the corresponding endpoint β_{RW}.

with $\langle X \rangle = 0$. In the vicinity of the RW transition line endpoints, B_4 with the finite size correction is a function of $x = (\beta - \beta_{RW})L_s^{1/\nu}$ and can be expanded as a series [5,17,18].

$$B_4 = B_4(\beta_c, \infty) + a_1 x + a_2 x^2 + \cdots. \tag{9}$$

In the thermodynamic limit, the critical index ν takes on the corresponding value summarized in Table I. $B_4(\beta_c, \infty)$ takes on the values 3, 1.5, 1.604, 2 for crossover, first order triple point, 3D Ising, and tricritical transitions, respectively. However, on finite spatial volumes, the steps of $B_4(\beta_c, \infty)$ are smeared out to continuous functions.

III. MC SIMULATION RESULTS

In this section, we first present the MC simulation parameters. The ϕ algorithm with a Metropolis accept/reject step is used [28]. The simulations are performed at

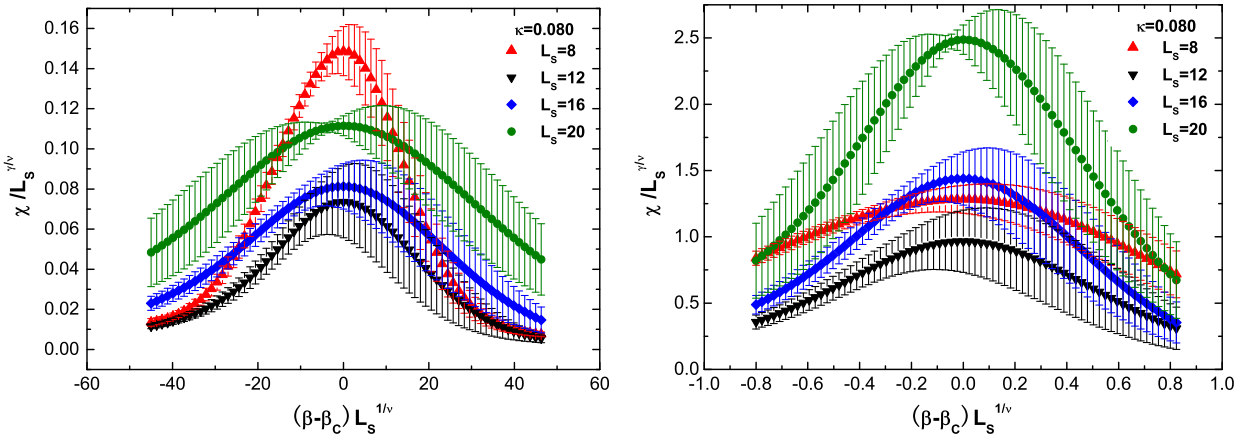

FIG. 3 (color online). Scaling behavior of the susceptibility of the imaginary part of the Polyakov loop according to the first order critical index (left panel), and to the 3D Ising critical index (right panel) at $\kappa = 0.080$.

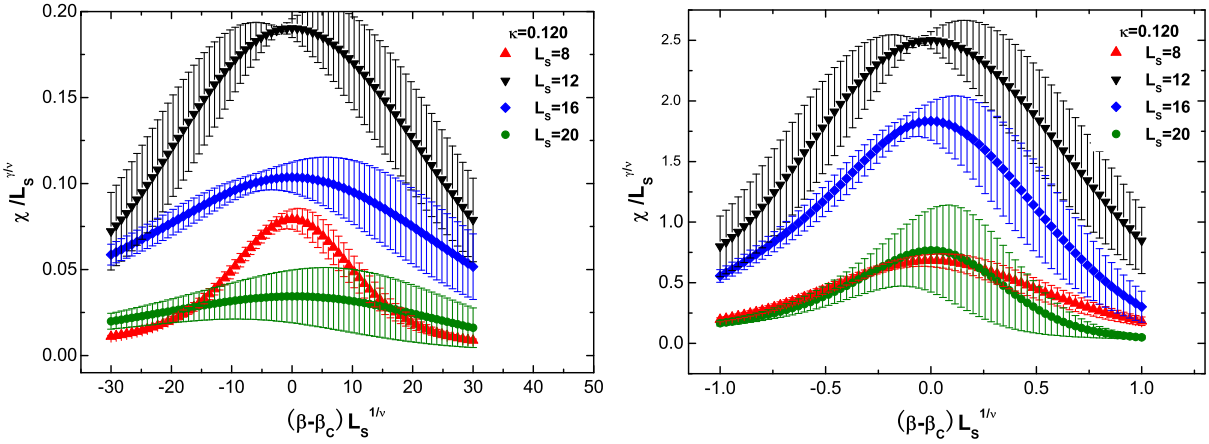

FIG. 4 (color online). Scaling behavior of the susceptibility of imaginary part of the Polyakov loop according to first order critical index (left panel), and to 3D Ising critical index (right panel) at $\kappa = 0.120$.

$\kappa = 0.020, 0.040, 0.060, 0.070, 0.080, 0.100, 0.120, 0.140$ on $L_t = 4$ lattice. For each κ value, lattices with spatial size $L_s = 8, 12, 16, 20$ are employed except at $\kappa = 0.140$ where simulations are carried out on lattice size $L_s = 8, 12$.

The acceptance rates range within 53%–95%. 20–50 molecular steps are taken for each trajectory. 20,000–100,000 trajectories are generated after 10,000–50,000 trajectories as warmup.

The conjugate gradient method is used to evaluate the fermion matrix inversion. For each lattice size, we make simulations at 4–11 different β values. In order to fill in observables at additional β values, we employ the Ferrenberg-Swendsen reweighting method [29].

The critical coupling β_{RW}'s on various spatial volume at different κ are summarized in Table II. These β_{RW}'s are determined from the locations of peak susceptibility of the imaginary part of the Polyakov loop.

We present the rescaling susceptibility of the imaginary part of the Polyakov loop $\chi/L_s{}^{\gamma/\nu}$ as a function of $(\beta - \beta_{RW})L_s^{1/\nu}$ in Fig. 1. At $\kappa = 0.020, 0.040$, the fermion mass is very large; the deconfinement transition behavior is expected to be mainly governed by the first order transition of the pure gauge system. However, from Fig. 1, we can find that $\chi/L_s{}^{\gamma/\nu}$ according to the first order transition index or the 3D Ising transition index at $\kappa = 0.040$ does not collapse with the same curve. The reweighted distribution of the imaginary part of the Polyakov loop presented in Fig. 2 which exhibits the one-state signal other than a weak two-state signal is not in favor of a first order transition. We cannot determine the nature of transition decisively based on the simulation results at $\kappa = 0.040$. At $\kappa = 0.020$, similar behavior is observed.

The rescaling behavior of $\chi/L_s{}^{\gamma/\nu}$ at $\kappa = 0.080$ and $\kappa = 0.120$ is presented in Figs. 3 and 4, respectively. From the two panels of Fig. 3, we can find that neither the first order transition index nor the 3D Ising transition index is suitable to describe the system at the RW transition endpoint. At $\kappa = 0.060, 0.070, 0.100, 0.120$ the rescaling observable $\chi/L_s{}^{\gamma/\nu}$ exhibits the similar behavior as that at $\kappa = 0.080$. For clarity, we only present the results at $\kappa = 0.120$ in Fig. 4.

In order to discern the scaling behavior at $\kappa = 0.060, 0.070, 0.080, 0.100, 0.120, 0.140$, we turn to investigate the Binder cumulant B_4 as defined in Eq. (8) whose scaling behavior is described in Eq. (9). B_4 decreases with the increase of β, and at one fixed κ value, B_4, as a function of β on various spatial volumes, is expected to intersect at one point. The intersection gives an estimate of an accurate location of β_{RW}. By fitting to Eq. (9), we can extract critical index ν, β_{RW} and $B_4(\beta_c, \infty)$. The results are collected in Table III. We present B_4 as a function of β at $\kappa = 0.080$, 0.120 in the left panels of Fig. 5, and B_4 as a function of $(\beta - \beta_{RW})L_s^{1/\nu}$ in the right panels of Fig. 5 with ν taken to be the extracted value through the fitting procedure. From

TABLE III. Results of critical couplings β_{RW} and the critical index ν by fitting Eq. (9) to data on different spatial volumes. The errors of β_{RW} are very small, so we take them to be zero.

κ	L_s	β_{RW}	ν	$B_4(\beta_c, \infty)$	a_1	a_2	r-square
0.060	8,12,16	5.6838(0)	0.3374(3)	2.3189(4)	−0.0793(5)	0.00127(1)	0.990
0.070	8,12,16	5.6812(0)	0.4187(2)	2.0745(3)	−0.289(8)	0.0244(2)	0.963
0.080	8,16,20	5.6753(0)	0.5872(4)	1.9747(3)	−1.272(4)	0.427(3)	0.977
0.100	8,12,16	5.6524(0)	0.5218(8)	1.8405(6)	−0.6956(56)	0.185(3)	0.995
0.120	8,12,16	5.6072(0)	0.6791(4)	1.7964(8)	−1.880(25)	1.364(36)	0.980
0.140	8,12	5.5428(21)	0.2222(2)	1.1853(4)	−0.0005(3)	0(0)	0.893

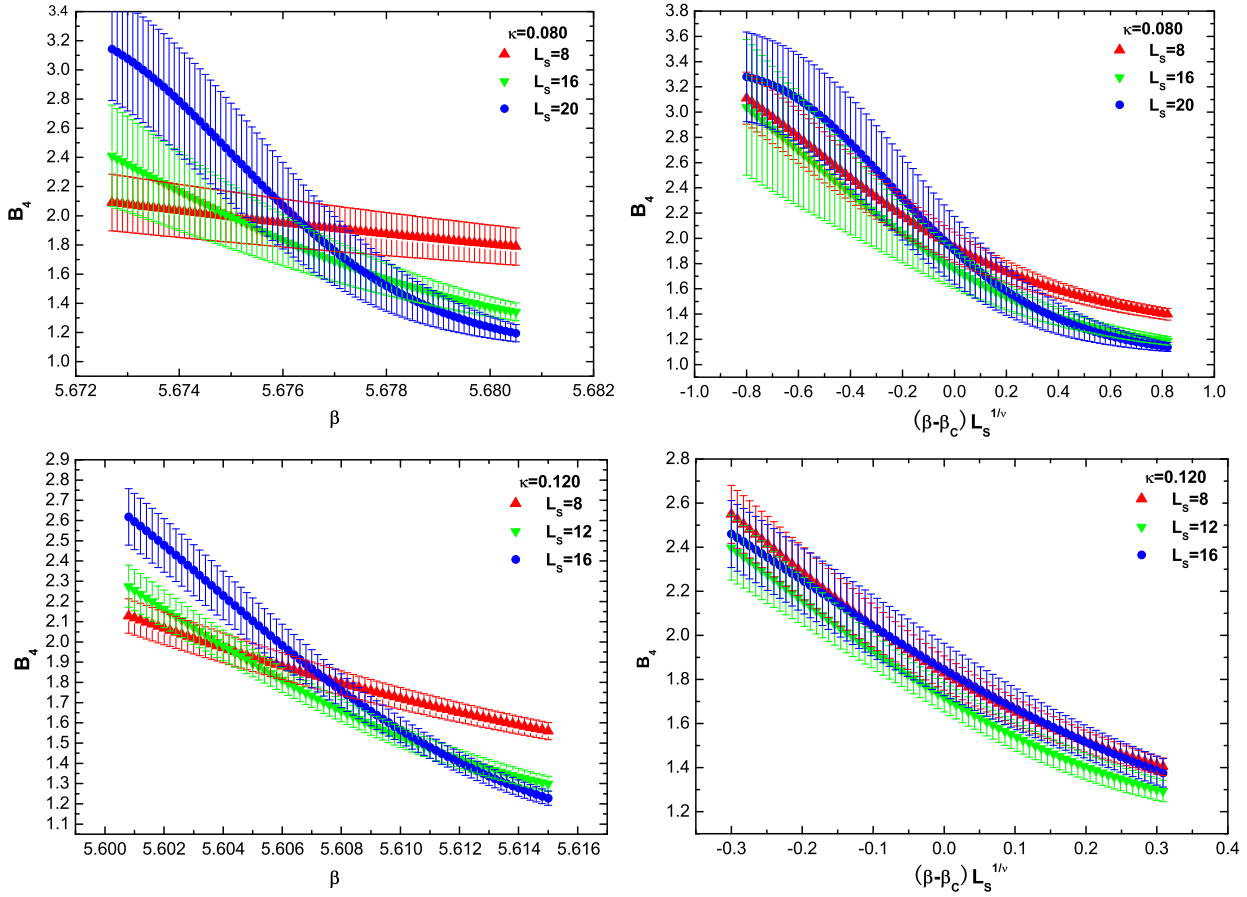

FIG. 5 (color online). Binder cumulants as a function of β on various spatial volumes intersect at one point (left panels), and as a function of $(\beta-\beta_c)L_s^{1/\nu}$ with values of β_c, ν from Table III collapse (right panels).

Table III, we find that the critical index ν at $\kappa = 0.080$, 0.100, 0.120 is larger than the value at the tricritical point.

From the values of ν in Table III, we conclude that the nature of the transition at $\kappa = 0.060$, 0.070 is of first order. The values of $B_4(\beta_c, \infty)$ at $\kappa = 0.060, 0.070$ are larger than the expected value. This is because logarithmic scaling corrections will be present near the tricritical point [5,30], and our simulations are carried out on the finite size volume on which large finite size corrections are observed

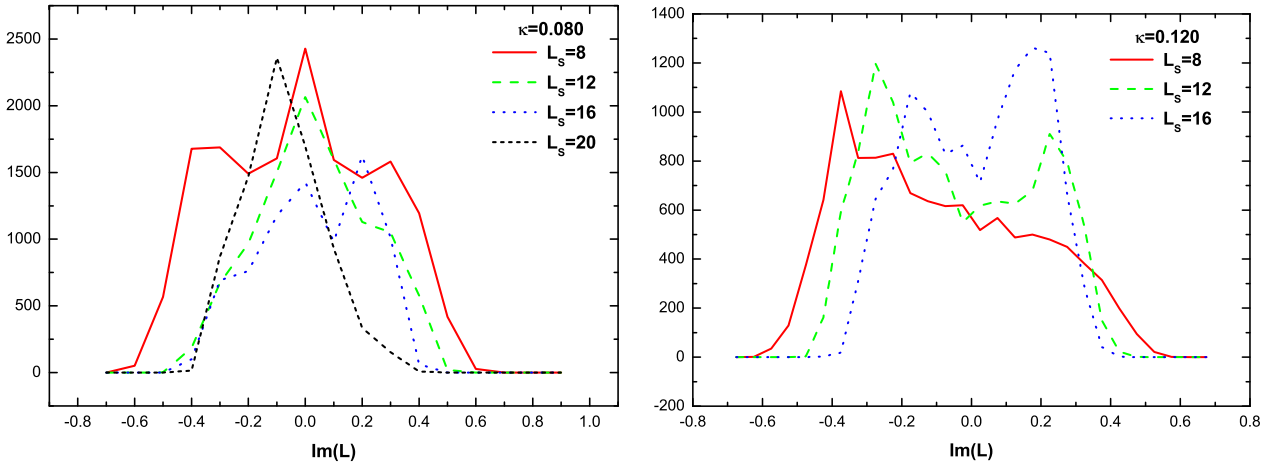

FIG. 6 (color online). Reweighted distribution of the imaginary part of the Polyakov loop at $\kappa = 0.080, 0.120$ at the corresponding endpoints β_c which are extracted by fitting.

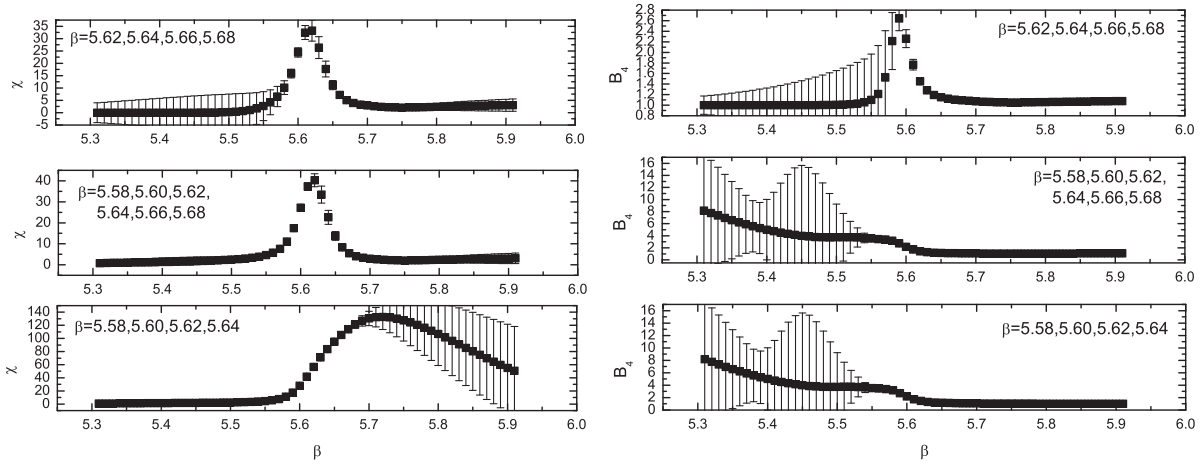

FIG. 7. Behavior of the susceptibility of the imaginary part of the Polyakov loop (left panels) and Binder cumulant (right panels) with a different selection of β values on $L_s = 8$ at $\kappa = 0.120$.

in simpler spin model [31]. However, the critical exponent ν is not sensitive to finite size corrections [5].

We also present the reweighted distribution of the imaginary part of the Polyakov loop at $\kappa = 0.080$, 0.120 in Fig. 6, from which we can find that the behaviors of the reweighted distribution of $\mathrm{Im}(L)$ are in favor of second order transition. The behavior of the reweighted distribution of $\mathrm{Im}(L)$ at $\kappa = 0.100$ is also checked.

Put our results with those in Ref. [26] together, we can estimate that the two tricritical points are between $0.070 < \kappa < 0.080$ and $0.120 < \kappa < 0.140$, and when $\kappa < 0.060$, our simulation results cannot enable us to determine the nature of transition decisively.

IV. DISCUSSIONS

We have studied the nature of critical endpoints of Roberge-Weiss transition of two flavor lattice QCD with Wilson fermions. When $i\mu_I = i\pi T$, the imaginary part of the Polayakov loop is the order parameter for studying the transition from the low temperature phase to the high temperature one.

In Ref. [25], Wilson fermions are employed to study the nature of RW transition endpoints. In Refs. [6,7] and Ref. [5], the simulations with staggered fermions show that the phase diagram of two flavor and three flavor QCD at imaginary chemical potential $i\mu_I = i\pi T$ is characterized by two tricritical points, respectively.

Our simulations are carried out at 8 values of κ on $L_t = 4$ lattice on different 4 spatial volumes. At each κ value, we take the β values in the reweighting procedure by monitoring the behavior of susceptibility of the imaginary part of the Polyakov loop. As an example, we present in Fig. 7 the behavior of χ and Binder cumulant B_4 with a different selection of β values on lattice $L_s = 8$ at $\kappa = 0.120$. From Fig. 7, we can find that the selection of $\beta = 5.58$, 5.60, 5.62, 5.64, 5.66, 5.68 may be the best. As a comparison, we present the results in the upper panels with $\beta = 5.62$, 5.64, 5.66, 5.68, and in the lower panels with $\beta = 5.58$, 5.60, 5.62, 5.64.

At $\kappa = 0.020$, 0.040, our simulations are not decisive for the determination of transition nature.

At $\kappa = 0.060$, 0.070, 0.080, 0.100, 0.120, 0.140, when the behavior of $\chi/L_s^{\gamma/\nu}$ is examined, it is difficult to decide the transition nature at the RW transition endpoint. We turn to investigate the Binder cumulant. By fitting Eq. (9) to our data, we can extract the values of critical index ν which are collected in Table III; the ν value at 0.060, 0.070, 0.140 supports that transition at the endpoints is of first order, whereas the ν value at 0.080, 0.100, 0.120 favors that the nature of transition is of second order.

By monitoring the change of ν at different κ values and comparing these values with those in the thermodynamic limit, we conclude that the tricritical points are between $0.070 < \kappa < 0.080$ and $0.120 < \kappa < 0.140$. However, this result is not in accord with the conclusion in Ref. [25] where Philipsen and Pinke believed that the two tricritical κ's are 0.100(9) and 0.155(5).

Considering the lattice volume in our simulations at $\kappa = 0.140$ is 8^3, 12^3, our result of the light tricritical point position is less reliable than that in Ref. [25]. Moreover, it is interesting that the position of the heavy tricritical point and some ν, β_{RW} values from our simulations are different from those in Ref. [25], in spite of the same regularization we employed as that used by Philipsen and Pinke.

We have no certain explanation for this disagreement; we speculate that it may be because of the different distribution around β_{RW} of those β values at which simulations are carried out. In Ref. [25], the β values are more concentrated around β_{RW} with $\Delta\beta = 0.001$, whereas, in our simulation, the β values are more scattered around β_{RW} with $\Delta\beta = 0.02$. Consequently, the β values we used cover a wider range. However, the less concentration of β values may lead us to lose much important information around

transition points, especially, when transition is under consideration. With limited calculation resources, it may be better that a more concentrated distribution of β values around transition points are used.

ACKNOWLEDGMENTS

We thank Philippe de Forcrand for valuable help. We modify the MILC Collaboration's public code [32] to simulate the theory at imaginary chemical potential. In some of our calculations, we use the fortran-90 based multi-precision software [33]. This work is supported by the National Science Foundation of China (NSFC) under Grants (No. 11105033, No. 11347029). The work was carried out at the National Supercomputer Center in Tianjin, and the calculations were performed on TianHe-1(A).

[1] K. Fukushima and T. Hatsuda, Rep. Prog. Phys. **74**, 014001 (2011).
[2] K. Fukushima, J. Phys. G **39**, 013101 (2012).
[3] J. B. Kogut and D. K. Sinclair, Phys. Rev. D **77**, 114503 (2008).
[4] C. Schmidt, *Proc. Sci.*, LAT2006 (2006) 021 [arXiv:hep-lat/0610116].
[5] P. de Forcrand and O. Philipsen, Phys. Rev. Lett. **105**, 152001 (2010).
[6] M. D'Elia and F. Sanfilippo, Phys. Rev. D **80**, 111501 (2009).
[7] C. Bonati, G. Cossu, M. D'Elia, and F. Sanfilippo, Phys. Rev. D **83**, 054505 (2011).
[8] M. D'Elia, F. Di Renzo, and M. P. Lombardo, Phys. Rev. D **76**, 114509 (2007).
[9] K. Nagata and A. Nakamura, Phys. Rev. D **83**, 114507 (2011).
[10] M. D'Elia and F. Sanfilippo, Phys. Rev. D **80**, 014502 (2009).
[11] P. de Forcrand and O. Philipsen, J. High Energy Phys. 01 (2007) 077.
[12] P. de Forcrand and O. Philipsen, J. High Energy Phys. 11 (2008) 012.
[13] L.-K. Wu, X.-Q. Luo, and H.-S. Chen, Phys. Rev. D **76**, 034505 (2007).
[14] Y. Sakai, H. Kouno, and M. Yahiro, J. Phys. G **37**, 105007 (2010).
[15] G. Aarts, S. P. Kumar, and J. Rafferty, J. High Energy Phys. 07 (2010) 056.
[16] H. Kouno, Y. Sakai, K. Kashiwa, and M. Yahiro, J. Phys. G **36**, 115010 (2009).
[17] O. Philipsen and P. de Forcrand, *Proc. Sci.*, LATTICE2010 (2010) 211 [arXiv:1011.0291].
[18] C. Bonati, P. de Forcrand, M. D'Elia, O. Philipsen, and F. Sanfilippo, *Proc. Sci.*, LATTICE2011 (2011) 189 [arXiv:1201.2769].
[19] A. Roberge and N. Weiss, Nucl. Phys. **B275**, 734 (1986).
[20] P. de Forcrand and O. Philipsen, Nucl. Phys. **B642**, 290 (2002).
[21] M. D'Elia and M.-P. Lombardo, Phys. Rev. D **67**, 014505 (2003).
[22] U. M. Heller, *Proc. Sci.*, LAT2006 (2006) 011 [arXiv:hep-lat/0610114].
[23] B. Bunk, M. Della Morte, K. Jansen, and F. Knechtli, Nucl. Phys. **B697**, 343 (2004).
[24] M. Golterman, Y. Shamir, and B. Svetitsky, Phys. Rev. D **74**, 071501(R) (2006).
[25] O. Philipsen and C. Pinke, Phys. Rev. D **89**, 094504 (2014).
[26] L.-K. Wu and X.-F. Meng, Phys. Rev. D **87**, 094508 (2013).
[27] A. Pelissetto and E. Vicari, Phys. Rep. **368**, 549 (2002).
[28] S. Gottlieb, W. Liu, D. Toussaint, R. L. Renken, and R. L. Sugar, Phys. Rev. D **35**, 3972 (1987).
[29] A. M. Ferrenberg and R. H. Swendsen, Phys. Rev. Lett. **63**, 1195 (1989).
[30] I. D. Lawrie and S. Sarbach, in *Phase Transitions and Critical Phenomena*, edited by C. Domb and J. L. Lebowitz (Academic Press, New York, 1984), Vol. 9.
[31] A. Billoire, T. Neuhaus, and B. Berg, Nucl. Phys. **B396**, 779 (1993).
[32] http://physics.utah.edu/~detar/milc/.
[33] http://crd-legacy.lbl.gov/~dhbailey/mpdist/.